

Short Communication

Engineering a Hierarchical Microtubular NiCoO₂ Architecture for Electrochemical Energy Storage Applications

Quande Che*, Fei Ma, Jingwen Wang, Ping Yang*

School of Materials Science and Engineering, University of Jinan, Jinan 250022, China

*E-mail: mse_cheqd@ujn.edu.cn (Q. Che), mse_yangp@ujn.edu.cn (P. Yang)

Received: 13 April 2020 / Accepted: 23 May 2020 / Published: 10 July 2020

This paper demonstrates a novel approach to prepare hierarchical mesoporous NiCoO₂ microtubes *via* a biomorphic mineralization technique by using natural cotton fibers as the template. As an anode material for lithium-ion batteries, the NiCoO₂ microtubes exhibited high reversible capacity, good rate capability, and outstanding cycle performance. Specifically, it delivered a reversible capacity of 603 mA h g⁻¹ at 200 mA g⁻¹ after 50 cycles and a capacity of 470 mA h g⁻¹ at 1200 mA g⁻¹. Importantly, the electrode exhibited a nearly stable cycling performance, with 85.3% capacity retention from 2–50 cycles at 200 mA g⁻¹ with approximately 98% coulombic efficiency. The impressive electrochemical performances can be attributed to two beneficial features of the as-prepared NiCoO₂ microtubes: the hollow porous structure and mesopores, which are accommodated the volume expansion and promoted Li-ion diffusion and electron transfer. Overall, the as-developed hierarchical microtubular mesoporous NiCoO₂ architecture is a prospect material for lithium ion batteries.

Keywords: Nickel cobalt oxides; Hierarchical microtubes; Mesoporous; Lithium ion batteries

1. INTRODUCTION

Lithium-ion batteries (LIBs) are a very important energy storage product that is widely applied in electronic equipment and new energy vehicles [1–3]. However, the growing demand for high power and high rate leads to increasing performance requirements. To date, carbonaceous materials are the dominant commercial anode, which obviously cannot satisfy the increasing requirements because of their relatively low specific capacity (theoretical value of 372 mA h g⁻¹) [4]. Thus, it is extremely necessary to explore alternative anodes for LIBs. Transition metal oxides (TMOs) have gained extensive attention as prospective candidates [5]. Among them, single-phase cobalt oxides and nickel oxides, such as CoO [6], Co₃O₄ [7], and NiO [8] have been widely investigated and exhibit good anodic performance.

Recently, in comparison to the characteristics of single TMOs, binary counterparts have been deemed to possess superior Li-ion diffusion, electron conductivity, cycling stability and mechanical stability [9]. It is thought that the two different metal cations in binary metal oxides have a synergistic effect. Therefore, binary TMOs, such as MnFe_2O_4 [10], ZnFe_2O_4 [11] and NiCo_2O_4 [12], have been investigated in depth as alternative materials for LIBs. Note that the main research focus is on the spinel structure, whereas nickel cobalt oxides other than NiCo_2O_4 (e.g., NiCoO_2) have not received enough attention. In particular, Ni^{2+} and Co^{2+} could form a NiO-CoO solid solution with the NaCl-type crystal structure, of which the two types of metal cations randomly occupy the 4a site. Both Ni and Co are electrochemically active metals compared to Li ions. Furthermore, previous studies demonstrated that NiO and CoO electrodes exhibited remarkable anodic performance [6,8]. Based on the above concerns, NiCoO_2 , i.e., a NiO-CoO solid solution, is an attractive anode material for high-performance LIBs.

Nevertheless, NiCoO_2 inevitably suffers the common problems of TMOs, such as low electric conductivity, inferior rate ability and poor cycle performance. Various methods have been evaluated to overcome these shortcomings based on two main scientific aspects: (i) the lithium-ion diffusion characteristics and electron-transfer kinetics and (ii) structural stability of the electrode materials. Constructing hierarchical porous structures is deemed to be an effective way to obtain high-performance LIBs [13,14]. In general, hierarchical structures assembled from elementary building blocks usually exhibit novel properties due to the synergistic effect of the construction units. Moreover, the porosity of the hierarchical structures can provide numerous interfacial contact areas with the electrolyte, shorten the Li-ion diffusion distance and greatly alleviate the volume expansion in the electrochemical process [15]. Many studies have been conducted to construct such hierarchical porous structures *via* approaches that include hydrothermal synthesis [16], template-assisted synthesis [17], and carbothermal reduction [18]. Zhu *et al.* reported a 3D hierarchical porous $\text{MnCo}_2\text{O}_4@\text{MnO}_2$ network that could retain a reversible capacity of 96% after 200 cycles at 100 mA g^{-1} [19]. Cao *et al.* also demonstrated the feasibility of obtaining a high energy capacity and good rate capability through engineering a hierarchical mesoporous bunched Co_3O_4 architecture [20]. Based on the above analysis, it is of great significance to construct NiCoO_2 with hierarchical mesoporous structural features that are beneficial to the electrochemical performance of LIBs.

Herein, hierarchical NiCoO_2 mesoporous microtubes were constructed as an anode material for LIBs *via* a biomimetic mineralization method. Specifically, the thermal decomposition of $\text{Ni}^{2+}/\text{Co}^{2+}$ cotreated natural cotton fibers in air directly generated NiCoO_2 mesoporous microtubes. The as-developed structure possesses several preferable characteristics: (i) the porosity of the hierarchical microtubes largely reduces the Li-ion diffusion distance; (ii) the microtubes assembled from small particles create an efficiently interconnected electron transport pathway along the longitudinal direction; and (iii) regarding the stability, the mesoporous structure provides structural ability against the strain that occurs during volume expansion. Electrochemical tests indicated that the as-developed hierarchical NiCoO_2 mesoporous microtubes are a promising material for LIBs.

2. EXPERIMENTAL

2.1 Materials synthesis

The hierarchical mesoporous NiCoO₂ microtubes were prepared *via* a biomorphic mineralization approach using natural cotton as a template. In a typical experiment, 0.05 mol of Ni(NO₃)₂·6H₂O and 0.05 mol Co(NO₃)₂·6H₂O were dispersed in 100 ml deionized water. Then the dried cotton fibers were added into the above solution and immersed for 48 h. After that the cotton fibers were dried at 60°C for 12 h. Finally, the product was obtained by sintering the treated cotton fibers at 900°C in air for 2 h.

2.2 Materials Characterization

X-ray powder diffraction (XRD) of the products was performed on a D8 Advance Bruker X-ray diffractometer with a Cu K α target. The morphologies of the samples were investigated *via* field emission scanning electron microscopy (FE-SEM, FEI, QUANTAFEG250). The Brunauer-Emmett-Teller (BET) specific surface area and pore size distribution were characterized by N₂ adsorption-desorption tests on an adsorption instrument (MFA-140).

2.3 Electrochemical measurements

Electrochemical tests were performed using CR2025-type coin cells. The electrodes were prepared by coating the slurry (80 wt% hierarchical mesoporous NiCoO₂ microtubes, 10 wt% carbon black, 10 wt% polyvinylidene fluoride (PVDF) binder dispersed in N-methyl-2-pyrrolidone (NMP) solvent on a Cu foil and drying it in a vacuum oven at 110 °C for 12 h. The coin cells were packaged in an Ar-filled glove box. Pure Li foil was used as the cathode. The electrolyte comprised 1.0 M LiPF₆ in a mixture of EC and DEC (1:1 volume). The charge-discharge measurements were conducted using a NEWARE battery tester (Shenzhen Neware Technology, China) over a range from 0.1–3 V (*vs.* Li⁺/Li). Cyclic voltammetry (CV) was performed on the CHI 660D electrochemical workstation at a scan rate of 0.1 mV s⁻¹ at room temperature.

3. RESULTS AND DISCUSSION

XRD was conducted to identify the crystal structure of the as-prepared samples. Fig. 1 shows the XRD pattern of the hierarchical porous NiCoO₂ microtubes. The diffraction peaks of the sample matched well to those for cubic CoNiO₂ (JCPDS 10-0188). This observation demonstrated that the Ni²⁺/Co²⁺ cotreated cotton fiber was decomposed and transferred into NiCoO₂ during the calcination process in air at 900°C. As seen from a graphic of the crystal structure set in the top right corner of Fig. 1, Ni²⁺ and Co²⁺ randomly occupy the 4a site of the NiCoO₂ cubic structure.

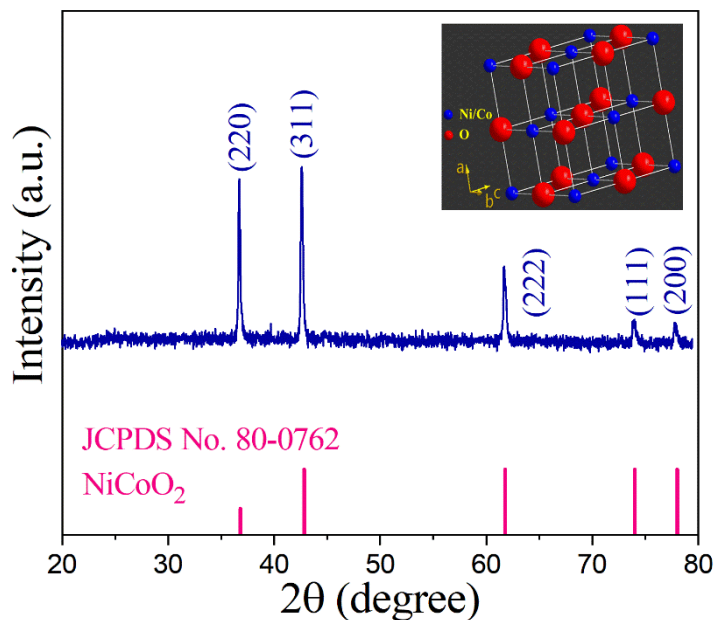


Figure 1. XRD pattern of the as-prepared hierarchical mesoporous NiCoO₂ microtubes. The set in top right corner is the corresponding graphic crystal structure representation.

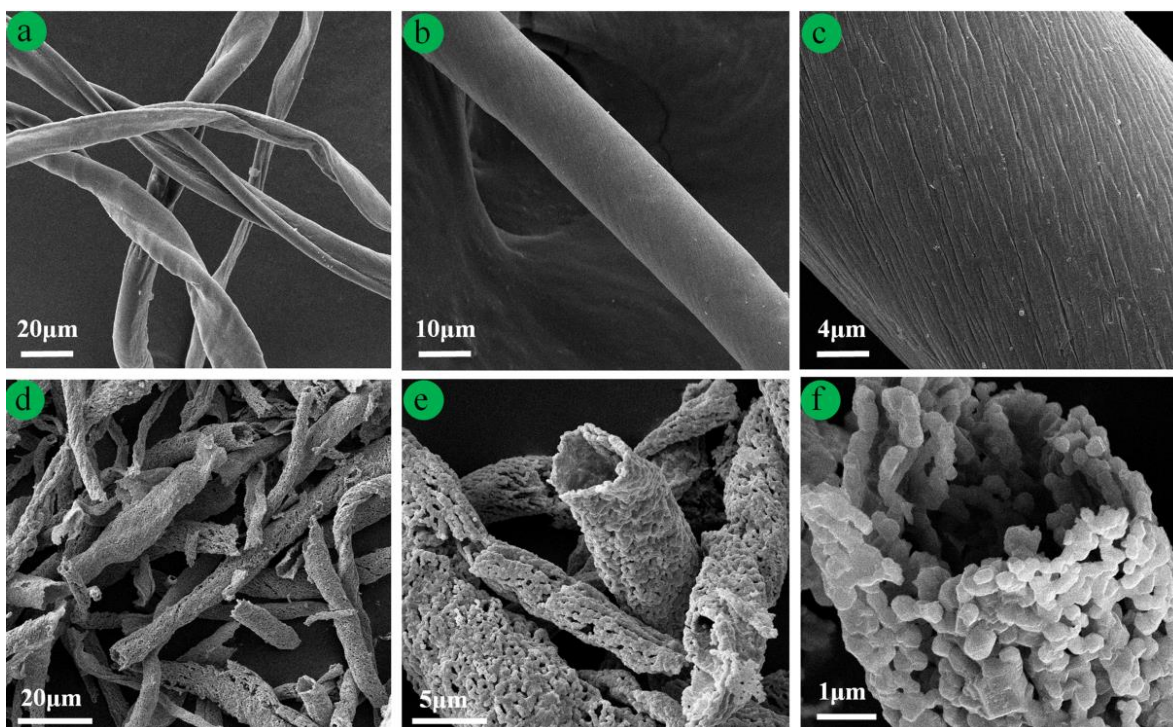


Figure 2. FESEM images of (a–c) cotton fibers and (d–f) NiCoO₂ microtubes at different magnifications.

The morphologies of the natural cotton fibers and the as-prepared NiCoO₂ microtubes were examined by FE-SEM, as shown in Fig. 2. In the low-magnification image (Fig. 2(d)), it can be seen that the as-prepared samples replicated the morphology of the cotton template well and exhibited a biomorphic structure. The high-magnification images (Fig. 2(e, f)) show that the as-obtained NiCoO₂

microtubes had a long and slender hollow structure with an inner diameter that ranged from 2–5 μm . Moreover, the NiCoO_2 microtubes were composed of small particles with an average size of 200 nm. Note that the small particles were interconnected and formed a hollow porous structure, which was favorable for the electrochemical performance of LIBs. This was especially true for the cycling performance because the preferable feature can enhance the structural stability.

Based on the experimental results from the XRD pattern and FE-SEM images, a possible formation mechanism of the NiCoO_2 microtubes can be proposed, as illustrated in Fig. 3. There are numerous surface hydroxyl groups on natural cotton fibers. Therefore, Ni^{2+} and Co^{2+} ions were adsorbed on the surface through electrostatic interactions. Then, the NiO and CoO crystal nuclei were formed *in-situ*. Subsequently, a NiO-CoO solid solution could be formed during the high-temperature sintering process. In addition, the formation of hollow porous structural features was due to the release of gases from the combustion of the cotton template, such as CO_2 , H_2O , and NO_2 .

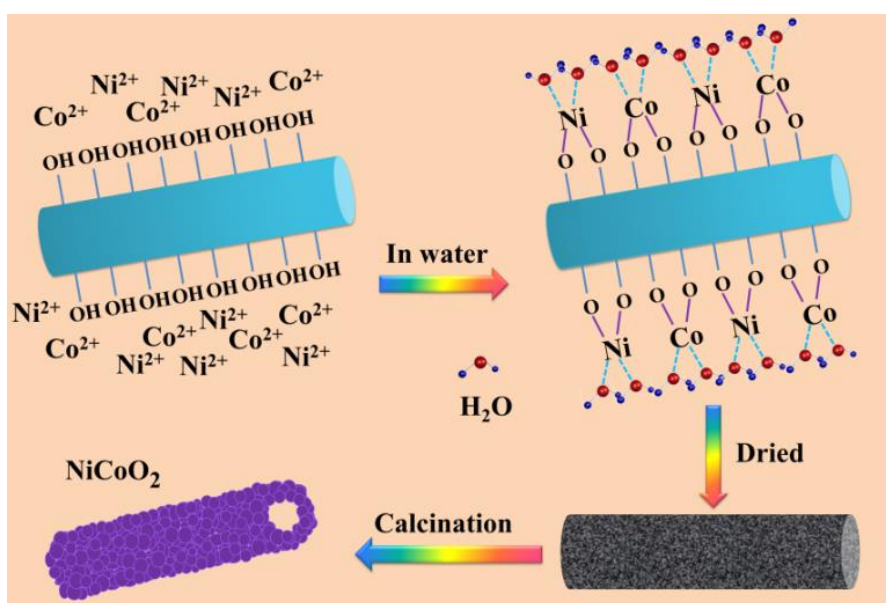


Figure 3. Schematic illustration of the fabrication procedure for the hierarchical mesoporous NiCoO_2 microtubes through biomimetic mineralization technique by using natural cotton fibers as template.

To study the porous structure and pore size distribution in the NiCoO_2 microtubes, BET measurements were performed, as shown in Fig. 4. The pore size distribution (set in Fig. 4) was calculated using the BJH method from the desorption curve of the isotherm. The calculated BET specific surface area of the NiCoO_2 microtubes was about approximately $27.4 \text{ m}^2 \text{ g}^{-1}$. A sharp peak at 2.6 nm and a wide peak located at 14.9 nm can be found at the pore-size distribution curve. Overall, the BET analysis confirmed the mesoporous nature of the NiCoO_2 microtubes, which is favorable for Li-ion diffusion and electrolyte transport during the electrochemical process.

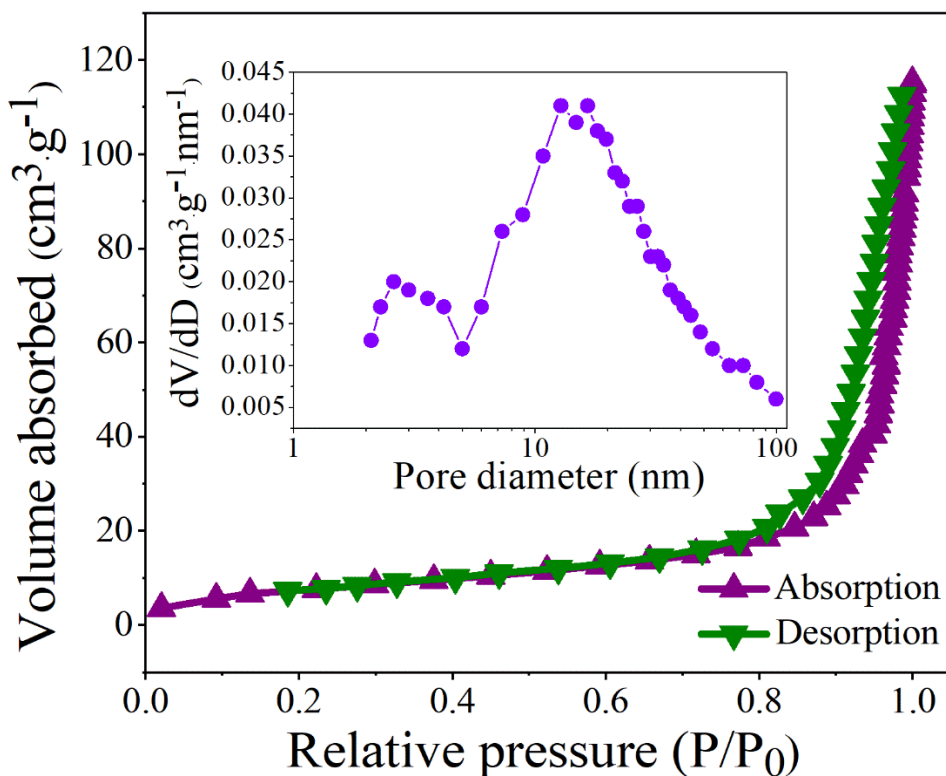


Figure 4. Nitrogen adsorption-desorption isotherms and the corresponding BJH pore-size distribution plots (inset) of the as-prepared NiCoO₂ microtubes. The pore-size distribution was determined from the desorption branch of the isotherms.

The electrochemical performance of the as-prepared hierarchical mesoporous NiCoO₂ microtubes was evaluated by galvanostatic charge-discharge cycling and CV at room temperature between 0.1 and 3.0 V versus pure Li metal. The charge-discharge profiles of the NiCoO₂ anode for the 1st, 2nd, 5th, 10th, and 50th cycles at a current density of 200 mA g⁻¹ are shown in Fig. 5 (a). The voltage profile of the 1st discharge electrochemical reaction exhibited a potential plateau from 0.63–0.75 V (*vs.* Li⁺/Li), while a potential plateaus from 2.0–2.30 V can be seen in the charge profiles, which is consistent with the previous report [21]. The first discharge and charge specific capacities of the NiCoO₂ electrode were 1068 mA h g⁻¹ and 725 mA h g⁻¹, respectively, with an irreversible capacity fading of 32.1%. The causes of such capacity fading are mainly the generation of a SEI layer and other secondary reactions. The discharge capacities of the NiCoO₂ electrode were 707 mA h g⁻¹, 682 mA h g⁻¹, 668 mA h g⁻¹ and 603 mA h g⁻¹ in the 2nd, 5th, 10th and 50th cycles, respectively. The charge-discharge capacity versus cycle number for up to 50 cycles is shown in Fig. 5(b). From the 2nd cycle onward, the NiCoO₂ electrode showed a nearly stable cycle performance, with an 85.3% capacity retention from 2–50 cycles. Moreover, the columbic efficiency was approximately 98% (2–50 cycles). The electrode still retained a reversible discharge capacity of 603 mA h g⁻¹ after 50 cycles. The enhanced cycling performance could be attributed to the intrinsic properties of the novel structure which greatly alleviated the volume expansion and promoted the diffusion of Li ions.

The rate performance of the as-prepared NiCoO₂ was also evaluated at various rates between 200 mA g⁻¹ and 1200 mA g⁻¹ and then back to 200 mA g⁻¹. As shown in Fig. 5(c), the NiCoO₂ anode delivered high discharge capacities of 700 mA h g⁻¹, 670 mA h g⁻¹, 590 mA h g⁻¹, and 526 mA h g⁻¹ when the current density changed stepwise from 200 mA g⁻¹ to 400 mA g⁻¹, 600 mA g⁻¹ and 1200 mA g⁻¹, respectively. More importantly, a high capacity of 613 mA h g⁻¹ was delivered again when the current rate was reduced from 1200 mA g⁻¹ back to 200 mA g⁻¹. The impressive electrochemical performance is comparable to or even superior to that of previous reports, as shown in Table 1.

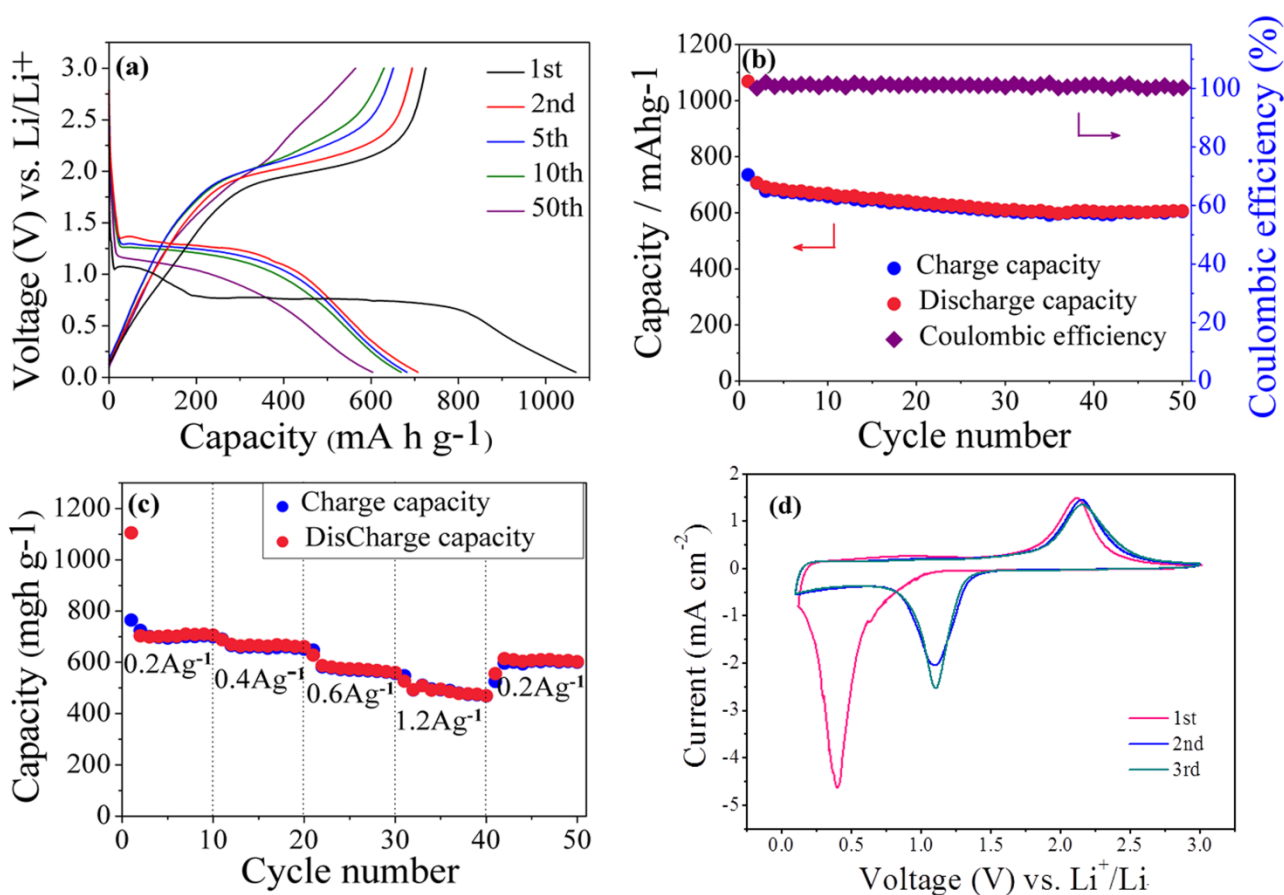


Figure 5. (a) Charge-discharge profiles for selected cycles of the as-prepared NiCoO₂ microtubes at a current density of 200 mA g⁻¹ in the voltage range of 0.1-3V at room temperature; (b) cycling performance of the NiCoO₂ electrode at a current density of 200 mA g⁻¹; (c) rate performance of the NiCoO₂ electrode at different current densities; (d) CV curves of the NiCoO₂ electrode at a scan rate of 0.1 mV s⁻¹ for the first three cycles.

Fig. 5 (d) shows typical CV curves of the first 3 cycles of the as-prepared NiCoO₂ electrode. In the first cycle, two reduction peaks occurred at approximately 0.38 V during the cathodic process, which correspond to the reduction of Co²⁺ to Co and Ni²⁺ to Ni in addition to the formation of Li₂O and a SEI layer [27]. The anodic peak at approximately 2.10 V is attributed to the oxidation from Co to Co²⁺ and Ni²⁺ to Ni in addition to the decomposition of Li₂O [28]. In the 2nd and 3rd cycles, the reduction peaks decreased and shifted to approximately 1.10 V, while the oxidation peaks slightly

shifted to 2.15 V. The redox reactions involved in the electrochemical process of the as-prepared NiCoO₂ mesoporous microtubes are as follows [29]:

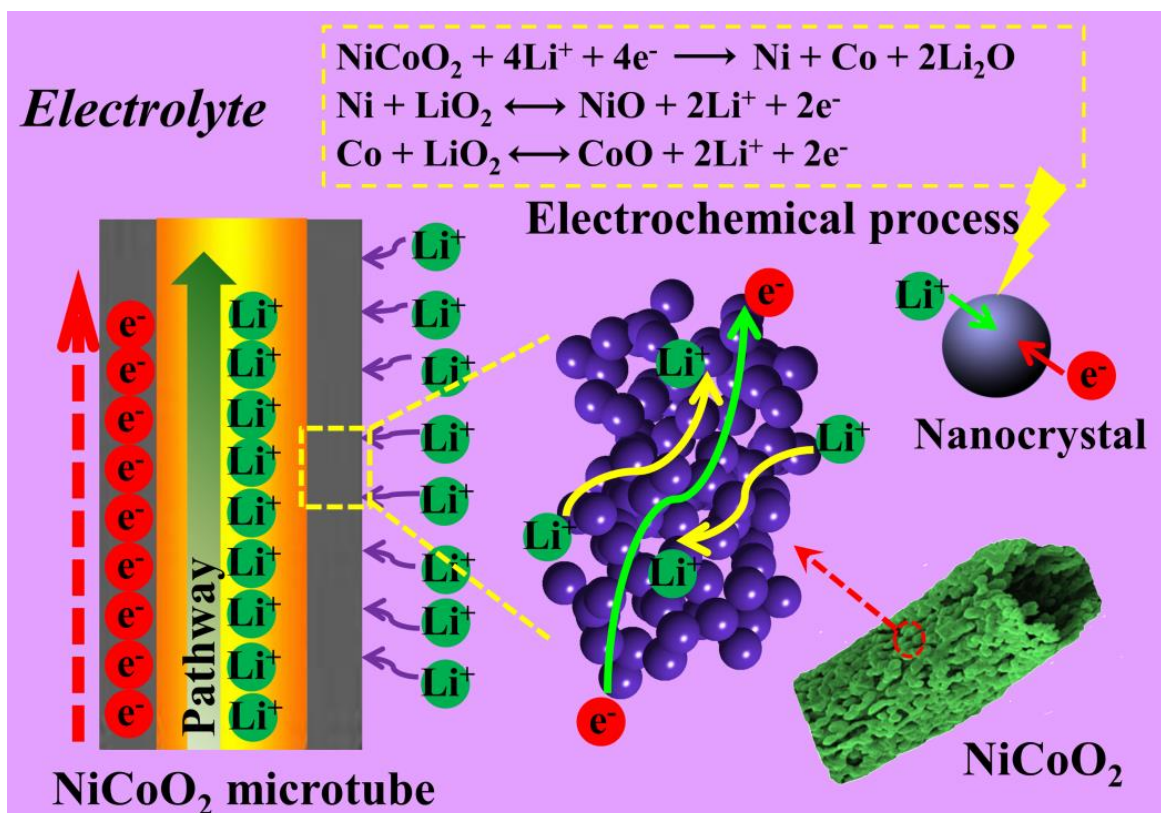
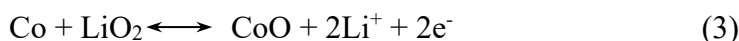
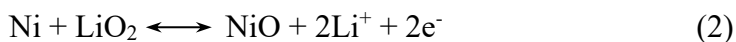
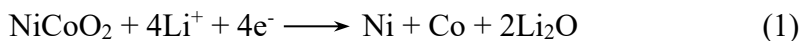


Figure 6. Schematic showing the as-prepared NiCoO₂ microtubes, simple representation of Li-ion diffusion and electron transfer paths in the electrode and the redox reactions involved of the electrochemical process.

Based on the above analysis, the impressive electrochemical performance of the NiCoO₂ microtubes was ascribed to the following several factors (Fig. 6). (i) The hollow porous architecture, namely, the open space, not only provide abundant active sites but also accommodate undesirable volume expansion, which is of importance for cycling stability. (ii) The hierarchical structure comprising of small particles provided a pathway along the longitudinal direction for electron transfer. (iii) The mesoporous structure largely reduced the Li-ion diffusion distance and provided numerous interfacial contact sites with the electrolyte. Therefore, the as-prepared hierarchical microtubular NiCoO₂ exhibited a high reversible capacity and good cycling performance.

Table 1. Summary of the electrochemical performance of the NiCoO₂ electrode reported in this work and similar reports.

Material	Current density (mA g ⁻¹)	Reversible capacity (mA h g ⁻¹)	Ref.
NiCoO ₂ microtubes (this work)	200	603 (50th)	Present work
	400	~660	
	600	~560	
	1200	~470	
NiCoO ₂ microflowers	100	~397 (50th)	[21]
	500	~326	
	1000	~228	
NiO-CoO nanospheres	200	~240 (50th)	[22]
Co-doped NiO	100	589.5 (50th)	[23]
CoO-NiO-C	100	268 (60th)	[24]
CoNiO ₂ hierarchical structure	100	449.3 (50th)	[25]
NiCoO ₂	-	716.5 (theoretical)	[26]

4. CONCLUSIONS

In summary, hierarchical mesoporous NiCoO₂ microtubes were developed through biomorphic mineralization techniques by using natural cotton fibers as the template. As an anode material for LIBs, this material exhibited a high reversible capacity, good rate ability, and outstanding cycle performance. It also delivered a 470 mA h g⁻¹ capacity at 1200 mA g⁻¹, and a high reversible capacity of 603 mA h g⁻¹ at 200 mA g⁻¹ after 50 cycles. The excellent electrochemical performance was ascribed to two beneficial features of the as-prepared NiCoO₂ microtubes: the hollow porous structure and mesopores, which accommodated volume expansion and promoted Li-ion diffusion and electron transfer. Overall, the excellent electrochemical performance, along with the novel and facile preparation process, make this a promising material for energy storage applications.

ACKNOWLEDGEMENT

The work was supported by the National Natural Science Foundation of China (51602128), the Research Foundation from University of Jinan (XKY1401, XBS1508, XBH1504).

References

1. W.D. Li, E.M. Erickson and A. Manthiram, *Nat Energy*, 5 (2020), 26.
2. K.Q. Ding, X.J. Gao, J.W. Han, X.M. He, R.L. Qu, L.J. Zhou, H.M. Dou, H. Wang and L. Wang, *Int. J. Electrochem. Sci.*, 15 (2020) 4684.
3. G. Lei and C.X. Xu, *Int. J. Electrochem. Sci.*, 15 (2020) 4434.

4. L. Croguennec and M.R. Palacin, *J. Amer. Chem. Soc.*, 137 (2015) 3140.
5. R.J. Clément, Z. Lun and G. Ceder, *Energy Environ. Sci.*, 13 (2020) 345.
6. C.C. Zhou, J.Z. Liu, S.Z. Guo, P.L. Zhang, S. Li, Y. Yang, J. Wu, L.Y. Chen and M.Y. Wang, *ChemElectroChem*, 7 (2020) 1573.
7. Y.J. Zhang, H.C. Yan, J.M. Liu, X. Li and Y.Y. Zhang, *Int. J. Electrochem. Sci.*, 15 (2020) 2894.
8. J. Fu, W.B. Kang, X.D. Guo, H. Wen, T.B. Zeng, R.X. Yuan and C.H. Zhang, *J. Energy Chem.*, 47 (2020) 172.
9. Y.J. Wang, Y.Z. Zhang, J.K. Ou, Q. Zhao, M. Liao and D. Xiao, *RSC Adv.*, 6 (2016) 547.
10. Z.H. Deng, M. He, Y.F. Feng and D.P. Xiong, *Int. J. Electrochem. Sci.*, 15 (2020) 4203.
11. P. Ren, Z. Wang, B.Q. Liu, Y.R. Lu, Z.S. Jin, L.Y. Zhang, L. Li, X.L. Li and C.G. Wang, *J. Alloy. Compd.*, 812, (2020) 152014.
12. C. Zhang, Z.H. Xie, W.F. Yang, Y. Liang, D.D. Meng, X. He, P. Liang and Z.H. Zhang, *J. Power Sources*, 451 (2020) 227761.
13. M. Chen, X.J. Jin, Z. Chen, Y.T. Zhong, Y.H. Liao, Y.C. Qiu, G.Z. Cao and W.S. Li, *J. Mater. Chem. A*, 7 (2019) 13120.
14. H.X. Yang, Y. Xie, M.M. Zhu, Y.M. Liu, Z.K. Wang, M.H. X and S.L. Lin, *Dalton Trans.*, 48 (2019) 9205.
15. Y.S. Li, J. Wang, Z.F. Zhou, Q.R. Yao, Z.M. Wang, H.Y. Zhou and J.Q. Deng, *Int. J. Electrochem. Sci.*, 14 (2019) 2822.
16. J. Li, M.L. Zhang, T.T. Xue, D.Y. Zhang, Y.X. Yan and Z.M. Li, *Int. J. Electrochem. Sci.*, 15 (2020) 587.
17. X.L. Ren, D.S. Ai, C.Z. Zhan, R.T. Lv, F.Y. Kang and Z.H. Huang, *Electrochim. Acta*, 318 (2019) 730.
18. H.J. Zhang, J.S. Shu, K.X. Wang, X.T. Chen, Y.M. Jiang, X. Wei and J.S. Chen, *J. Mater. Chem. A*, 2 (2014) 80.
19. Y.D. Zhu, Y. Huang and M.Y. Wang, *Chem. Eng. J.*, 378 (2019) 122207.
20. Y. Xiao, C.W. Hu and M.H. Cao, *J. Power Sources*, 247 (2014) 49.
21. Y.G. Liu, Y.Y. Zhao, Y.L. Yu, M. Ahmad and H.Y. Sun, *Electrochim. Acta.*, 132 (2014) 404.
22. X. Xu, B.T. Dong, S.J. Ding, C.H. Xiao and D.M. Yu, *J. Mater. Chem. A*, 2 (2014) 13069.
23. Y.J. Mai, J.P. Tu, X.H. Xia, C.D. Gu and X.L. Wang, *J. Power Sources*, 196 (2011) 6388.
24. Y.F. Wang and L.J. Zhang, *J. Power Sources*, 209 (2012) 20.
25. X. Xu, B. Dong, S. Ding, C. Xiao and D. Yu, *J. Mater. Chem. A*, 2 (2014) 13069.
26. Y.M. Wang, X. Zhang, C.Y. Guo, Y.Q. Zhao, C.L. Xu and H.L. Li, *J. Mater. Chem. A*, 1 (2013) 13290.
27. X.H. Wang, L. Qiao, X.L. Sun, X.W. Li, D.K. Hu, Q. Zhang and D.Y. He, *J. Mater. Chem. A*, 1 (2013) 4173.
28. Y.H. Wei, F.L. Yan, X. Tang, Y.Z. Luo, M. Zhang, W.F. Wei and L.B. Chen, *ACS Appl. Mater. Interfaces*, 7 (2015) 21703.
29. Z.D. Huang, K.Z. Zhang, T.T. Zhang, X.S. Yang, R.Q. Liu, Y. Lia, X.J. Lin, X.M. Feng, Y.W. Ma and W. Huang, *Energy Storage Mater.*, 3 (2016) 36.